Historical sand injections on the Mediterranean shore of Israel: evidence for liquefaction hazard

Shmuel Marco, Oded Katz & Yehoshua Dray

Natural Hazards
Journal of the International Society for the Prevention and Mitigation of Natural Hazards

ISSN 0921-030X
Volume 74
Number 3

Nat Hazards (2014) 74:1449-1459
DOI 10.1007/s11069-014-1249-6

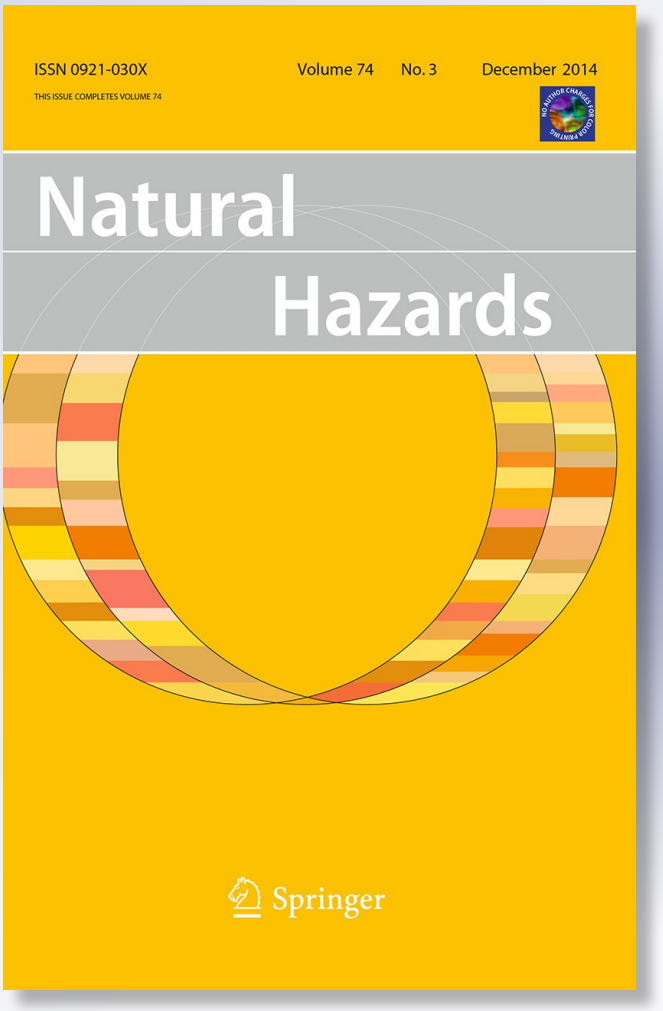

Springer

Nat Hazards (2014) 74:1449–1459
DOI 10.1007/s11069-014-1249-6

ORIGINAL PAPER

Historical sand injections on the Mediterranean shore of Israel: evidence for liquefaction hazard

Shmuel Marco · Oded Katz · Yehoshua Dray

Received: 26 July 2013 / Accepted: 18 May 2014 / Published online: 30 May 2014

Abstract The abundant silt and sand along the coastal plain of Israel have long been considered susceptible to liquefaction, but previous searches have failed to find field evidence for it. We report the first finding of typical liquefaction features and silty sand injections in trenches that were excavated behind a fourth century Byzantine dam on the Taninim Creek, some 850 m inland of the Mediterranean shore. The trenches revealed a series of flame-shape injections of silty sand that penetrate the overlying clay-rich soil. The injections are largest and most frequent within several meters of the point where the dam is badly damaged on the seaward side, which we interpret as a possible result of a large wave. Three features make the sand injections special: (1) their lower extent is commonly asymmetric with dominant southeastward vergence, away from the breach in the dam, (2) zigzag shapes characterize the upper parts of many injections, and (3) the size and frequency of the injections diminish gradually with distance from the dam until they completely disappear some 100 m away from it. We suggest that the sand injections can be explained by overpressure that was induced either directly by earthquake shaking or by a tsunami wave that breached the dam, filled the reservoir behind the dam and increased the pressure on the water-saturated silt and sand layers and triggered liquefied sand injections. The movement of water sloshing back and forth in the lake accounts for the zigzag shape of the injections. The similarity to structures that were observed in Thailand after the great 2004 tsunami and other palaeotsunami observations lead us to prefer the tsunami origin of the liquefaction features. Based on the stratigraphic position, the archeological context, and

S. Marco (✉)
The Department of Geophysical, Atmospheric, and Planetary Sciences,
Tel Aviv University, Tel Aviv, Israel
e-mail: shmulikm@tau.ac.il

O. Katz
Geological Survey of Israel, Jerusalem, Israel
e-mail: odedk@gsi.gov.il

Y. Dray
Restoration of Ancient Technology, Binyamina, Israel
e-mail: yeshu@netvision.net.il

the historical accounts, we suggest that an earthquake of November 25, 1759 is the most plausible trigger of the sand injections, either directly or via earthquake-induced tsunami. The observations demonstrate the vulnerability of the densely populated coastal plain to liquefaction.

Keywords Sand injections · Liquefaction · Earthquakes · East Mediterranean · Archeoseismology · Tsunami

1 Introduction

The majority of the population in Israel lives along the coastal plain, a narrow (<15 km) stripe up to 60 m above sea level. The coastal plain is where our study area is located. It is mostly covered by loose sand and soil, bounded by the seashore on the west and by low hills, mostly consisting of Late Cretaceous limestone and other carbonates, on the east.

Earthquake hazards that may threaten the population along the coastal plain include direct damage from shaking, earthquake-triggered liquefaction, and tsunami waves. The most plausible sources of earthquakes in the region are the Dead Sea Fault (DSF), which lies some 60–100 km east of the coastal plain (Fig. 1), and the Carmel Fault, probably a branch of the DSF (Shamir et al. 2001). The N–S-striking linear shoreline led Neev et al. (1973) to suggest that it is also a tectonic, fault-related feature. Deep faults, which are evident only in seismic reflections, in addition to sedimentary facies changes, led Garfunkel and Derin (1984) to suggest a Triassic breakup that shaped the continental passive margin in it present position (see also Garfunkel 2004). The reactivation of these faults is uncertain. Minor faults in the Late Pleistocene sandstone units have been reported as well (Bakler et al. 1985; Sivan and Galili 1999; Sivan et al. 1999). The claim of faulting activity along the coast is challenged by Sneh (2000), whose re-examination of structural, stratigraphic, sedimentologic, geomorphologic, and archeological observations led to the conclusion that the only tectonic activity in the coastal plain involves regional emergence and submergence movements. It is of utmost importance to determine the seismic hazards that might threaten the densely populated coastal plain. Even if no coastal zone faults are active, history shows that strong onshore DSF earthquakes are capable of triggering submarine slump-related tsunamis that can hit the Levant coastline (Fokaefs and Papadopoulos 2007; Salamon et al. 2007). In addition, an extensive survey of the liquefiable deposits in Israel (Salamon et al. 2008) shows that the present study area of the coastal plain is susceptible to liquefaction, which $M > 6$ earthquakes along the DSF are highly likely to trigger, but no such earthquake-triggered liquefaction has been found to date.

The coastal plain is characterized by shore-parallel elongate valleys separated by Late Pleistocene to Holocene quartz eolianite sandstone ridges, locally called "Kurkar" (Sivan et al. 1999). These ridges also are apparent offshore in a multibeam swath mapping (Sade et al. 2006). Stream channels and Creeks such as the Taninim Creek (Fig. 1), which originate at the chalk and limestone hills on the east, cut across the Kurkar ridges on their way to the sea, forming gaps in the otherwise continuous ridges. In the past, the limited drainage gave rise to marshes in the valleys, part of which were drained in the Roman era some two millennia before present by excavated passages and tunnels to let the water out and reclaim land for agriculture. The silt and calcarenite deposited in the marshes are of the silty-sandy grain size, and their loose packing makes them susceptible to liquefaction.

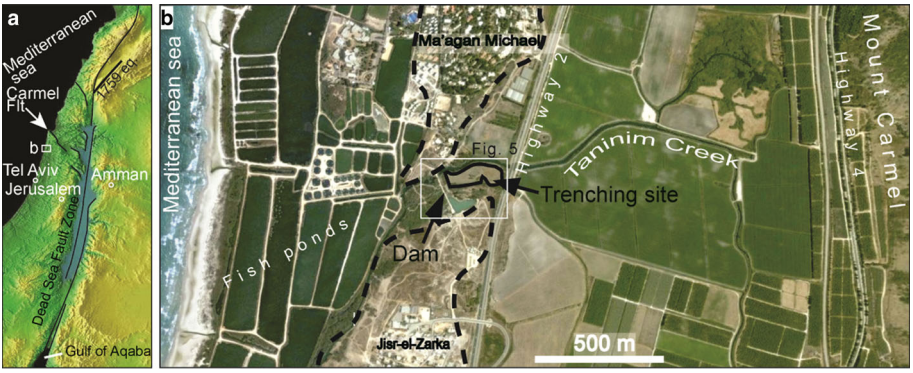

Fig. 1 **a** A general location map showing the Dead Sea Fault (*solid black lines*). **b** A Google Earth image of the Taninim Creek area. *Dashed lines* delineate the eolianite sandstone ("Kurkar") ridge, which is cut by the Taninim Creek between the settlements of Kibbutz Maagan Michael and Jisr el Zarka

Similarly, the quartz sand that is transported by longshore current from the Nile Delta is liquefiable (Salamon et al. 2008).

The other earthquake-triggered hazard on the coastal plain is tsunami. Historical accounts of tsunami waves that have hit the coasts of the eastern Mediterranean are reviewed by Salamon et al. (2007), who list a total of 23 reliable accounts since the fourteenth century BCE. The only geological evidence for an historical tsunami is reported from offshore Caesarea, where a layer rich in mollusk shells and shreds of ceramics is interpreted as backwash from the Roman harbor of Caesarea (Reinhardt et al. 2006), and another layer with high content of coarse grains is attributed to tsunami waves produced during the Late Bronze Age eruption of Santorini (Goodman-Tchernov et al. 2009).

Despite deliberate searches, no evidence for liquefaction nor for tsunami is known from onshore observations, possibly because of the intensive human activity in modern times that have obliterated or concealed them.

We set out to search for such evidence in sheltered undisturbed environments. One such place is a stretch of lake sediments that accumulated behind a historical dam on the Taninim Creek (Figs. 1, 2). The Creek drains the calcareous hills of the southern Carmel Mountain and the eastern flanks of Samaria and crosses the shore-parallel eolianite ridge on its way to the sea. The narrow crossing was used to build a dam for storing water, possibly for flushing sand out of the harbor of Caesarea. We found that laminated white calcareous sand and silt transported from the east were deposited on top of older clay-rich layer at the bottom of the water reservoir (Fig. 2). A layer of younger, massive, clay-rich soil overlies the laminated calcareous sand. The sandy shore west of the dam consists of quartz grains that are transported by along-shore current from the Nile delta (Zviely et al. 2007).

2 Dam history

The dam on the Taninim Creek (Fig. 2), which was built by the Byzantines in the fourth century CE as an artificial reservoir, was part of a flushing mechanism to clear silt from the Caesarea harbor, and for operating vertical flourmills as a by-product. The dam that is

Fig. 2 Photographs: **a** View of the dam looking northeastward. **b** A closeup view of the damaged section at the northern end of the dam. Building stones are shifted eastward (*arrows*) as if hit from the west. **c** and **d** Load structures were formed by liquefaction of the lower light-colored lacustrine silt that penetrated the overlaying dark clayey soil. We interpret the structure asymmetry and zigzag shapes as result of shear forces exerted on the lakebed sediments by waves sloshing back and forth

preserved along 193 m was originally more than 300 m long, 5.5 m wide at the base, and 4.5 m wide at the top. The top of the dam is 7 m above mean sea level.

A shallow fresh-brackish water lake was formed on the eastern side of the dam. Porat (2002) argues that the system was in use at least until the mid-sixth century, based on evidence from the "Christian Building", which received its water from the "Lower Aqueduct", a drinking-water carrier (bypassing the dam system) to Caesarea. After the Arab conquest in 640 CE, all the external water sources of Caesarea ceased to operate, included the studied dam reservoir. The inhabitants instead used water from wells that were dug in almost every house, as was told by the historian Al Mukadasi (cited by Porat 2002). However, a series of Ottoman flourmills powered by water from the dam reservoir indicate much later activity, possibly through the eighteenth century. We therefore argue that the lake persisted until the late Ottoman period.

A tilt of 7° from the vertical, leaning eastward (top moved eastward), most probably because of foundation settling, was fixed already in the dam's early days. We recognize a late occurrence of damage at the dam's northern end, where a 10-m section of the western face is destroyed; the upper part of the dam is missing, and the remaining stones are shifted eastward (Fig. 2b). A plausible explanation for the damage is that a large wave hit the dam, most intensely on its northern end. Later, the dam was repaired in the Ottoman period, when a massive support wall was built on the eastern face of the breached section, doubling the thickness of that part of the dam, and a series of 11 flour mills were built on the

west side of the dam (Peleg 2002). We interpret the repair as supporting evidence for the operational condition of the dam when it was hit (Fig. 2). The spillways of the Ottoman flourmills were opened in the dam lower than the watermark of the fourth century CE, possibly because the damaged dam could not hold the lake water at the original level.

3 Sedimentary and palaeoseismic observations

In search for clues for palaeoseismic deformation, we documented five backhoe-excavated 1.5-m-deep trenches (T1–T5) and one archeological excavation bank (T6) east of the fourth century Byzantine dam in the area that was occupied by the artificial lake. We found exactly the same stratigraphy in all the sections (Fig. 3), which we divide into four units. The lowest strata consist of pre-dam gray-brown clayey soil (we were unable to expose its base because of groundwater that prevented deeper trenching). It is overlain by a 0.8–1.0-m thick sequence of laminated, whitish, calcareous sand, silt, and some clay. The third unit is a 0.5-m darker sequence of light-brown 0–0.15 m silt and clay mixture with abundant fossils and 0.4-m light-brown massive clay-rich soil with carbonate concretions (up to 2 cm in diameter) and shell fragments (0.5 cm). The uppermost unit is a dark brown soil, but it is within the agricultural zone.

The second unit is therefore enclosed between two clay beds of low permeability, which act as seals that prevent fluid escape. This stratigraphy makes the second unit vulnerable to liquefaction. Grain-size analysis shows that the lake sediments (unit 2) from the trenches are mostly silt (mode is 3–39 microns) with sand content of up to 11 %.

Similar laminated sequences are reported from the Dead Sea Basin, where deposition rates of the order of 1 mm/yr are estimated (Schramm et al. 2000; Waldmann et al. 2009). Based on the accumulation of the laminated lake deposits in the studied lake sediments, and assuming that they represent annual cycles typical to the regional climate of dry rainless summers and wet rainy winters, the time equivalent is in the range of 1,000–1,300 years.

We sampled all the units in the section and found that all 10 samples contain fresh-brackish water gastropods, mostly *Melanopsis,* as well as *Theodoxus, Mienisiella, Bithynia, Melanoides, Phytia, Bulinus, Planorbis*, and *Radix*. All the samples also contain typical fresh-brackish water ostracodes. A single specimen of marine foraminifera (*Pullenia*) found in sample TN-9 was probably washed into the lake with floodwater from the east.

We interpret the lower whitish laminated silt as fresh-to-brackish water deposits of the artificial lake, which was formed behind the dam after it was built in the fourth century. The clay-rich top-soil unit reflects the pedogenic processes, which could start when the lake had dried; hence, the sharp lithological boundary is dated to circa eighteenth century. The abundant *Melanopsis* shells in the lower brown clay indicate frequent freshwater environment. We found only one dateable piece of detrital organic matter in sample TN8 that yielded a ^{14}C age 250 ^{14}C yrs BP, in agreement with the other data (Fig. 3).

At the boundary between the lake sediments and the topsoil layer, we discovered a series of flame structures that we interpret as injections, where the silty sand is intruded into the dark soil strata (Fig. 2). We documented 30 such structures along a 13-m traverse on the southern wall of trench T-1, 56 structures along a 20-m traverse on eastern wall of trench T-3, and 7 along 3 m on the eastern wall of T5 (Table 1). Many injections have zigzag shapes. The height of the injection structures is about 30 cm on the northwest side of the lake, close to the break in the dam, and it becomes smaller away from the dam toward the southeast. In T5, the injections are only up to 5 cm, and in T6, the easternmost

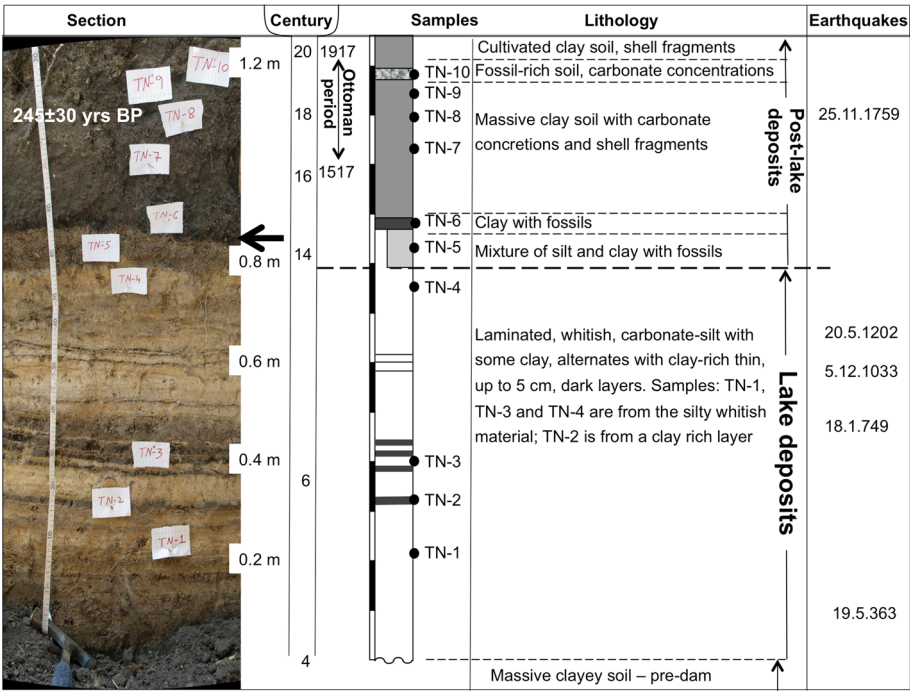

Fig. 3 Columnar section of the sediments in a trench east of the dam. The photograph mosaic on the left shows the location of samples. *Arrow* shows the horizon where flame structures are observed (Fig. 2). A single ^{14}C age of detrital charcoal from TN8 is 245 ± 30 BP. The earthquakes that were associated with tsunamis according to historical accounts are listed. The temporal constraints imposed on the observed sedimentary section and the correlation with the archeological stratigraphy indicate that the liquefaction and the damage to the dam occurred after the deposition of the laminated lake sediments and accumulation of some 30 cm of clayey soil, and before the construction of the flourmills toward the end of the Ottoman period. The earthquake of November 25, 1759 is the most plausible cause for these features

trench, there are no such structures at all and the sediment is undisturbed. The lower parts of most of the injections are strongly asymmetric. We counted 14 injections in T-1 and 42 injections in T-3; the dominant vergence is eastward (12 out of 14 injections in T-1) and southeastward (29 out of 42 injections in T-3), but north- and west-verging structures are also observed. The upper parts of the zigzag injections do no not exhibit uniform vergence (Fig. 2). The vergence and the liquefaction size gradient are summarized in Fig. 4.

4 Discussion

The sand injections may be interpreted as the result of overpressure in the lacustrine deposits, which could have been triggered either by earthquake shaking or by a sudden increase of overburden (Trifunac 1995). We examine these two possibilities in light of the observations detailed above.

Liquefaction and sand injections are often reported in association with earthquakes (Obermeier 2009). Since no evidence for active faulting is found along the coast, we argue that the source of the causative earthquake was remote. The possible sources are the

Table 1 Summary of injection structure characteristics in studied trenches (Fig. 3)

Trench	Length (m)	Wall	Liquefaction direction				Height (cm)
			E[a]	W[a]	Symmetric[b]	Multi[c]	
T1	13	S	12	2	16	–	5.3 ± 1.7
			S[a]	N[a]	Symmetric[b]	Multi[c]	
T3	20	E	29	10	14	3	10.1 ± 5.6
T5	3	E	4	–	2	–	12.7 ± 4.4

[a] Injection structure with one direction

[b] Injection or wave structure

[c] Injection structure with changing directions

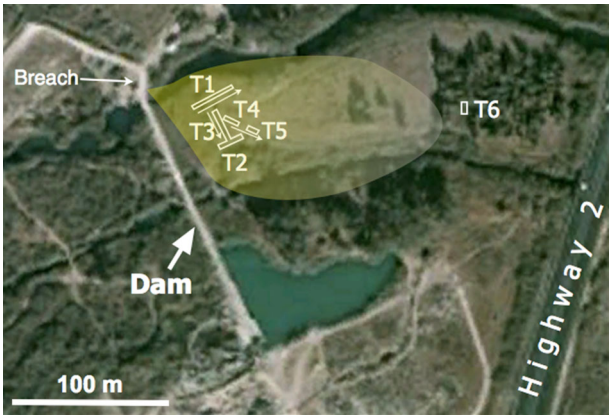

Fig. 4 The transport directions deduced from the flame structures asymmetry (*white arrows*) and schematic liquefaction intensity gradient (*yellow overlay*) showing decreasing intensity toward the east

Carmel Fault, about 25 km northeast, or the Dead Sea Fault, about 60 km east of Taninim, both capable of generating $M > 6$ earthquakes (e.g., Arieh 1967; Hamiel et al. 2009; Hofstetter et al. 2007). Compilations of liquefaction–epicentral distance data from Italy and eastern Mediterranean regions (Galli 2000; Papathanassiou et al. 2005) show that an $M \sim 6$ earthquake on the Carmel Fault or $M > 6.5$ earthquake at the Dead Sea Fault is capable of triggering liquefaction in our study area. The earthquake history of the Carmel Fault is not well known, but observations on a meticulously built Medieval basilica located on top of the fault, which does not exhibit any earthquake-related damage, indicate that during the last eight centuries there was no significant earthquake along it (Marco et al. 2006). Hence, we conclude that the source was along the Dead Sea Fault. An $M > 6.5$ on the Jordan Valley segment or an $M > 7$ on either the northern or the southern segments are plausible. Hence, earthquake-induced liquefaction is a possible cause for the flame structures observed in the study site.

The conspicuous, nearly uniform asymmetry of the injection structures here (Fig. 3) is rare in other occurrences of injected sand. Earthquake-related sand injections are commonly symmetrical, upright, exhibiting upward-directed flow features (e.g., Obermeier 2009; Tuttle and Schweig 1995). We therefore hypothesize that the asymmetry may have

been caused by shear that was induced by dominant southeastward flow, and the zigzag shapes at the upper parts of many injection structures indicate the sloshing of water back and forth. The flow could trigger shear instability at the upper part of the sediment, also known as Kelvin–Helmholtz Instability (Drazin and Reid 2004). Palaeotsunamis have been reported to trigger sand injection features, e.g., by De-Martini et al. (2003) and Owen and Moretti (2011), and asymmetric flame structures were observed in the deposits of the December 26, 2004 tsunami in Thailand (Matsumoto et al. 2008). The latter describe asymmetric injections of fine sand that was deposited by the tsunami, which intrude the overlying coarse-grained strata, uniformly skewed in the direction of the run-up current. Matsumoto et al. (2008) interpret the sequence as a result of two tsunami waves, where the boundary between the two deposited strata, i.e., the top of the first wave deposits, was simultaneously deformed and truncated by the second run-up current. Another set of asymmetric folds and injections observed in cores from the Aysén Fjord, Chile were associated with mass movement triggered by the April 27, 2007 Mw 6.2 earthquake (Van Daele et al. 2013). In the Lisan Formation (the palaeoDead Sea sediments), similar zigzag-shaped injections are capped by fragmented laminae. The sequence is interpreted as the result of re-suspension of the bottom sediment by the shear with the water during seiche or tsunami events (Alsop and Marco 2012; Wetzler et al. 2010). We suggest that a rapid addition of about 3 m of water (measured from the lake deposits to the top of the dam) during a tsunami surge could increase the overburden on the sandy layer, which is confined at its bottom and top with stiff clayey soil. The surge would have induced a sudden increase of pressure of 0.3 bars, at least three times the confining pressure (assuming soil thickness were similar to that of present, i.e., about 0.5 m and bulk density of about 1.5 g/cc). These conditions are highly likely to trigger liquefaction and the injection of water-saturated sediment into the overlying soil (Trifunac 1995). This scenario is somewhat similar to the case of palaeotsunami deposits that were found in the Kakawis Lake, near the shore of the Vancouver Island, British Columbia (Lopez 2012). We did not find deposits of marine origin, either because of the intensive modern agricultural cultivation of the upper strata that mixed the soil and made the microfossils very rare and hard to find, or because seawater did not go over the dam. An alternative tsunami-related explanation for the liquefaction on the eastern side of the dam could be a pressure gradient developed by increasing water head on the western side of the dam, where the tsunami wave ramped up but did not top the dam entirely (Craig 2004). While this mechanism and the earthquake-induced mechanism may explain why we have not found marine fauna east of the dam, it does not explain the systematic asymmetry of the injection structures.

We therefore argue that the observed injections of the sand were triggered by an earthquake, and the shape of the injections combined with the damage at the seaward face of the dam favor the involvement of a tsunami wave.

The candidate-triggering events are the earthquakes that postdate the accumulation of the entire sequence of lake deposits and some 20–30 cm of clay-rich soil that was formed at the surface after the lake dried.

The historical accounts that associate tsunamis with earthquakes in this region have been reviewed and screened for reliability (Salamon et al. 2011, 2007), but none of the reliably recorded ones stands out as having a significant run-up that could top the 7-m-high dam (possibly 1–2 m less at the breached section). The precise location of the shoreline in the past is unknown, but it may have been different, shore transport along the coast of Israel following the construction of modern ports and marinas (Zviely et al. 2007). In the absence of local active faults, the tsunamis can be induced by remotely triggered submarine slumps (Salamon et al. 2007). We cannot determine independently the precise age

of the observed liquefaction; however, the most suitable trigger candidate according to the dam history presented above, and the single ^{14}C age, is the earthquake of November 25, 1759 (Fig. 3). Reports on this catastrophic earthquake describe boats that were swept ashore from the Akko harbor (50 km north of the studied site), and a large wave that was reported from as far south as the Nile Delta (Ambraseys and Barazangi 1989). The 90-km-long surface rupture of this earthquake was reported by the contemporary French Consul to Beyrouth after visiting the site in Lebanon (Ambraseys and Barazangi 1989) and confirmed by palaeoseismic studies (Daëron et al. 2005; Gomez et al. 2001). Ambraseys and Barazangi (1989) estimate the earthquake magnitude at 7 plus.

5 Conclusions

The injections of silty sand found at the interface between the artificial lake sediments and the overlying clay-rich dark soil demonstrate, for the first time as field-observation, the vulnerability of the coastal plain sediments to liquefaction that may be triggered by earthquakes either on the Carmel Fault or on the Dead Sea Fault. Archeological age constraints make the earthquake of November 25, 1759 at the northern DSF the most likely trigger of the liquefaction in the Taninim reservoir deposits. Based on the asymmetry of the injections, their diminishing size away from the dam, the associated damage to the seaward face of the dam, and the resemblance to modern analogues, we prefer the tsunami surge overpressure as the probable mechanism inducing the liquefaction at the study site: an earthquake-triggered tsunami hit the dam, damaged its northern section, and rapidly added about 3 m of water to the reservoir. The elevated overburden-induced sand injections that became asymmetric because of the shear induced by the flow of water from the breached part of the dam toward the southeast. If this scenario is correct, in addition to historical accounts, we now have field observations that demonstrate the vulnerability of the eastern Mediterranean coast to tsunamis.

Acknowledgments Yael Edelman-Furstenberg and Ahuva Almogi of the Geological Survey of Israel are thanked for performing micro- and macropalaeontology analyses. We thank Rivka Amit (Geological Survey of Israel) for the grain size analysis and Neta Wechsler (TAU) for performing the ^{14}C dating. Thorough reviews by journal referees Ian G Alsop and Eugene (Buddy) Schweig helped us to significantly improve the manuscript. We are grateful for the generous cooperation and assistance of the staff in the Nahal Taninim National Park. The research was supported by the Israel Science Foundation grant #1736/11 to SM.

References

Alsop GI, Marco S (2012) Tsunami and seiche-triggered deformation of offshore sediments. Sed Geol 261–262:90–107

Ambraseys NN, Barazangi M (1989) The 1759 earthquake in the Bekaa valley: implications for earthquake hazard assessment in the eastern Mediterranean region. J Geophys Res 94(B4):4007–4013

Arieh EJ (1967) Seismicity of Israel and adjacent areas. Isr Geol Surv Bull 43:1–14

Bakler N, Neev D, Magaritz M (1985) Late Holocene tectonic movements at Tel-Haraz Southern Coast of Israel. Earth Planet Sci Lett 75(2–3):223–230

Craig RF (2004) Craig's soil mechanics. Spon Press, New-York

Daëron M, Klinger Y, Tapponnier P, Elias A, Jacques E, Sursock A (2005) Sources of the large AD 1202 and 1759 near East earthquakes. Geology 33(7):529–532

De-Martini PM, Burrato P, Pantosti D, Maramai A, Graziani L, Abramson H (2003) Identification of tsunami deposits and liquefaction features in the Gargano area (Italy): paleoseismological implication. Ann Geophys 46(5):883–902

Drazin PG, Reid WH (2004) Hydrodynamic stability. Cambridge University Press, New York, p 626
Fokaefs A, Papadopoulos GA (2007) Tsunami hazard in the Eastern Mediterranean: strong earthquakes and tsunamis in Cyprus and the Levantine Sea. Nat Hazards 40(3):503–526
Galli P (2000) New empirical relationships between magnitude and distance for liquefaction. Tectonophysics 324(3):169–187
Garfunkel Z (2004) Origin of the Eastern Mediterranean basin: a reevaluation. Tectonophysics 391(1–4):11–34
Garfunkel Z, Derin B (1984) Permian-early Mesozoic tectonism and continental margin formation in Israel and its implications for the history of the Eastern Mediterranean. Geol Soc, Lond, Spec Publ 17(1):187–201
Gomez F, Meghraoui M, Darkal AN, Sbeinati R, Darawcheh R, Tabet C, Khawlie M, Charabe M, Khair K, Barazangi M (2001) Coseismic displacements along the Serghaya fault: an active branch of the Dead Sea Fault System in Syria and Lebanon. J Geol Soc 158:405–408
Goodman-Tchernov BN, Dey HW, Reinhardt EG, McCoy F, Mart Y (2009) Tsunami waves generated by the Santorini eruption reached Eastern Mediterranean shores. Geology 37(10):943–946
Hamiel Y, Amit R, Begin ZB, Marco S, Katz O, Salamon A, Zilberman E, Porat N (2009) The seismicity along the Dead Sea Fault during the last 60,000 years. Seismol Soc Am Bull 99:2020–2026. doi:10.1785/0120080218
Hofstetter R, Klinger Y, Amrat AQ, Rivera L, Dorbath L (2007) Stress tensor and focal mechanisms along the Dead Sea fault and related structural elements based on seismological data. Tectonophysics 429(3–4):165–181
Lopez GI (2012) Evidence for mid- to late-Holocene palaeotsunami deposits, Kakawis Lake, Vancouver Island, British Columbia. Nat Hazards 60(1):43–68
Marco S, Agnon A, Ussishkin D, Finkelstein I (2006) Archaeoseismic observations in the Carmel fault zone: Megiddo versus Yoqne'am. In: Kessel R, Kagan E, Porat N (eds) Israel geological society annual meeting, Israel Geological Society, Bet Shean, p 79
Matsumoto D, Naruse H, Fujino S, Surphawajruksakul A, Jarupongsakul T, Sakakura N, Murayama M (2008) Truncated flame structures within a deposit of the Indian Ocean Tsunami: evidence of syn-sedimentary deformation. Sedimentology 55(6):1559–1570
Neev D, Bakler N, Moshkovi S, Kaufman A, Magaritz M, Gofna R (1973) Recent faulting along Mediterranean Coast of Israel. Nature 245(5423):254–256
Obermeier SF (2009) Using liquefaction-induced and other soft-sediment features for paleoseismic analysis. In: McCalpin, JP, ed. Paleoseismology, 62 Academic Press, San Diego, pp 497–564
Owen G, Moretti M (2011) Identifying triggers for liquefaction-induced soft-sediment deformation in sands. Sed Geol 235(3–4):141–147
Papathanassiou G, Pavlides S, Christaras B, Pitilakis K (2005) Liquefaction case histories and empirical relations of earthquake magnitude versus distance from the broader Aegean region. J Geodyn 40(2–3):257–278
Peleg Y, (2002) The dams of Caesarea's low-level aqueduct, *in* Amit, D, Patrich, J, and Hirschfeld, Y, (eds) The Aqueducts of Israel, 46 Portsmouth, Journal of Roman Archaeology, Supplementary Series, Rhode Island, pp 141–147
Porat Y, (2002) The water-supply to Caesarea: a re-assessment, *in* Amit D, Patrich J, and Hirschfeld Y, (eds) The Aqueducts of Israel, Volume 46: Portsmouth, Rhode Island, Journal of Roman Archaeology, Supplementary Series, pp 104–129
Reinhardt EG, Goodman BN, Boyce JI, Lopez G, van Hengstum P, Rink WJ, Mart Y, Raban A (2006) The tsunami of 13 December A.D. 115 and the destruction of Herod the Great's harbor at Caesarea Maritima, Israel. Geology 34(12):1061–1064
Sade AR, Hall JK, Amit G, Golan A, Gur-Arieh L, Tibor G (2006) The Israel national bathymetric survey—a new look at the seafloor off Israel. Isr J Earth Sci 55:185–187. doi:10.1560/IJES_55_3_185
Salamon A, Rockwell T, Ward SN, Guidoboni E, Comastri A (2007) Tsunami hazard evaluation of the eastern Mediterranean: historical analysis and selected modeling. Bull Seismol Soc Am 97(3):705–724
Salamon A, Zviely D, Rosensaft M, Lehmann T, Heimann A, Avramov R (2008) Zones of required investigation for liquefaction hazard in the coastal plain of Israel. Isr Geol Survey GSI/34/2008
Salamon A, Rockwell T, Guidoboni E, Comastri A (2011) A critical evaluation of tsunami records reported for the Levant Coast from the second millennium BCE to the present. Isr J Earth Sci 58:327–354. doi:10.1560/IJES.58.2-3.327
Schramm A, Stein M, Goldstein SL (2000) Calibration of the ^{14}C time scale to 50 kyr by ^{234}U-^{230}Th dating of sediments from Lake Lisan (the paleo-Dead Sea): earth Planet. Sci Lett 175:27–40

Shamir G, Bartov Y, Sneh A, Fleisher L, Arad V, Rosensaft M (2001) Preliminary seismic zonation in Israel. The Geological Survey of Israel and the Geophysical Institute of Israel, GII550/95/01(1) and GSI12/2000

Sivan D, Galili E (1999) Holocene Tectonic Activity in the Coastal and Shallow Shelf of the Western Galilee Israel, a Geological and Archaeological Study. Isr J Earth Sci 48:47–61

Sivan D, Gvirtzman G, Sass E (1999) Quaternary stratigraphy and paleogeography of the Galilee coastal plain Israel. Quaternary Res 51(3):280–294

Sneh A (2000) Faulting in the coastal plain of Israel during the Late Quaternary, reexamined. Isr J Earth Sci 49(1):21–29

Trifunac MD (1995) Empirical criteria for liquefaction in sands via standard penetration tests and seismic wave energy. Soil Dyn Earthq Eng 14(6):419–426

Tuttle MP, Schweig ES (1995) Archaeological and pedological evidence for large prehistoric Earthquakes in the New-Madrid Seismic Zone Central United-States. Geology 23(3):253–256

Van Daele M, Cnudde V, Duyck P, Pino M, Urrutia R, De Batist M (2013) Multidirectional, synchronously-triggered seismo-turbidites and debrites revealed by X-ray computed tomography (CT). Sedimentology 61:861–880. doi:10.1111/sed.12070

Waldmann N, Stein M, Ariztegui D, Starinsky A (2009) Stratigraphy, depositional environments and level reconstruction of the last interglacial Lake Samra in the Dead Sea basin. Quatern Res 72(1):1–15

Wetzler N, Marco S, Heifetz E (2010) Quantitative analysis of seismogenic shear-induced turbulence in lake sediments. Geology 38(4):303–306

Zviely D, Kit E, Klein M (2007) Longshore sand transport estimates along the Mediterranean coast of Israel in the Holocene. Mar Geol 238(1–4):61–73